CrystEngComm

Accepted Manuscript

ROYAL SOCIETY OF CHEMISTRY

www.rsc.org/crystengcomm

Journal Name

RSCPublishing

ARTICLE

Flux method growth of bulk MoS_2 single crystals and application as a saturable absorber

Cite this: DOI: 10.1039/x0xx00000x

Xixia zhang,[1]Fei Lou,[1]Chunlong Li,[1]Xiang Zhang,[1] Ning Jia,[1]Tongtong Yu,[1] Jingliang He,[1,2]Baitao Zhang,[1,2]Haibing Xia,[1,2]Shanpeng Wang,[1,2*]and Xutang Tao[1,2*]

Received 00th January 2012,
Accepted 00th January 2012

DOI: 10.1039/x0xx00000x

www.rsc.org/

Molybdenum disulfide (MoS_2) has attracted a great deal of attention because of its outstanding physical, chemical and optoelectronic properties. The method used to prepare large sized MoS_2 crystals of very high quality is still an important issue for determining the feasibility of its application. Herein, we propose a novel Sn flux method to grow single crystal MoS_2, and bulk MoS_2 single crystals with a size of 3 mm × 5 mm were successfully obtained by using a cooling rate of 2-4 °C/h. The growth mechanism of the MoS_2 crystal in Sn flux was investigated in detail using optical microscopy and atomic force microscopy (AFM). The obvious screw dislocation steps that are revealed suggest that the growth of MoS_2 is controlled by a screw-dislocation-driven (SDD) spiral growth mechanism. The flux-grown MoS_2 crystals were exfoliated to produce high-quality large-scale films using the liquid-phase exfoliation method. Using ultrathin MoS_2 films as a saturable absorber, a passively Q-switched laser at a wavelength of 1.06 μm was constructed and operated, with a narrow pulse width of 326 ns.

Introduction

Recently, layered transition metal dichalcogenides (TMDCs) with formula MX_2 (M = Mo, W; X = S, Se, and Te) have attracted a great deal of attention due to their unique properties.[1-3] These interesting properties make them promising candidates for applications in electronics,[4] optoelectronic devices,[5, 6] energy storage devices,[7, 8] and electrocatalysis.[9] MoS_2 is a representative layered TMDC. It consists of stacked covalently coupled S-Mo-S sheets, with adjacent layers connected by weak van der Waals forces. The indirect bandgap of bulk MoS_2 is 0.89-1.2 eV，while monolayer MoS_2 has a direct bandgap of 1.8 eV.[4, 10, 11] So far, much research effort has been devoted to MoS_2 in focusing on the preparation[12-17] of few-layered MoS_2 and its applications. Excellent crystal quality and a large surface area are important to realize the applications of ultrathin MoS_2 films.[18, 19] Ultrathin MoS_2 sheets can be obtained through scotch-tape exfoliation[4], lithium-based intercalation[13] or liquid-phase exfoliation[20] from commercially available, naturally occurring MoS_2 crystals or MoS_2 powder. Recently, chemical vapor deposition (CVD)[18, 21] has also been used to directly grow large-area monolayered or few-layered MoS_2 crystals. However, the two types of method still have shortcomings for obtaining MoS_2 films. MoS_2 films obtained by the former method are relatively small, while those grown by the latter method usually exhibit some defects. Therefore, the way to obtain large-area and highly crystalline MoS_2 ultrathin layers is still a critical issue. However, there are very limited literatures on the growth of bulk single MoS_2 crystals, which has a significant effect on the scale and crystallinity of ultrathin MoS_2 films. Ubaldini et al. reported the growth of bulk TMDCs crystals by chemical vapor transport method.[22] H. J. SCHEEL[23] reported that alkali polysulfides were flux suitable for the preparation of many metal sufides, including $NaCrS_2$, CdS, FeS_2 , MoS_2 etc. In addition, very recently, MoS_2 films have been found to hold promise for use in optoelectronic applications. For example, there are some reports on Q-switched and mode-locked laser operation of fiber lasers using MoS_2.[24-26] In the field of solid state lasers (SSLs), Wang et al.[11] studied the broadband saturable absorption of MoS_2 prepared by pulsed laser deposition (PLD); and Xu et al.[27] reported on a passively Q-switched laser using sub-micron scale MoS_2 sheets as the saturable absorber. In order to achieve higher pulse peak power and pulse energy, further investigation should be carried out on the saturable absorption properties of high quality MoS_2 single crystals especially in SSLs. Large-scale high-quality MoS_2 sheets would exhibit more advantages in the complex SSLs.

In this work for the first time, to the best of our knowledge，large-sized high-quality bulk MoS_2 single crystals with dimensions of 3 mm×5 mm were grown by the Sn flux method. The MoS_2 crystals develop with a screw-dislocation-driven (SDD) growth mechanism, as supported by the observation of screw dislocation steps on the surface of the crystals. From the as-grown MoS_2 crystals, high-quality and large-scale ultrathin MoS_2 samples were obtained by liquid-phase exfoliation. Using the ultrathin MoS_2 sheets, we experimentally demonstrated the photonics application of the MoS_2 SA for passive Q-switching operation, with nanosecond pulses of width 326 ns that were successfully generated at an operational wavelength of 1.06 μm.

Experimental section

Sn flux method growth of MoS_2

High purity elemental molybdenum (2N), sulfur (5N), and tin (5N) were used as the starting materials, and were loaded into a quartz ampoule which was evacuated to 2.0×10^{-3} Pa. It was then sealed off. The quartz ampoule containing the starting materials was placed into a single-temperature-zone coil furnace controlled by a temperature controller (SHIMADEN FP23). Typically, the heating program of the furnace was set as follows: slow heating to 1100-1150 °C and holding at this temperature for 25 h to ensure complete melting; the furnace was then cooled to 1000 °C at a rate of 0.5 - 6 °C/h, and maintained for 20 h to allow the crystals to grow; the growth ampoule was then drawn out of the furnace at 1000 °C. The ampoule containing the melt was then centrifuged for 3 minutes at a speed of 1500 r/min. It is necessary to move quickly during the entire drawing and centrifuging process in order to maintain the crystallization morphology that occurs at 1000°C. Bulk MoS_2 single crystals were obtained after the Sn flux was diluted in concentrated hydrochloric acid.

Preparation of ultrathin MoS_2

MoS_2 bulk crystals were exfoliated using the convenient and widespread method of liquid-phase exfoliation. The MoS_2 crystals (0.003g) were put into a centrifuge tube filled with 1.5 mL ethyl alcohol, then the centrifuge tube was sonicated in a KQ3200 ultrasonic cleaner, at a power of 120 W and ultrasonic frequency of 40 Hz. After 3 hours, the resultant dispersions were rotated in a centrifuge for 10 min at a rate of 12000 rpm. The supernatant was decanted into another container.

Characterization

Powder X-ray diffraction was performed with a Bruker-AXS D8 ADVANCE X-ray diffractometer equipped with a diffracted beam monochromator set for Cu Kα radiation (λ = 1.54056 Å) over the range of 10–80 °(2θ), with a step size of 0.02 ° and a step time of 0.04 s at room temperature. A Laue diffractometer manufactured by Multiwire Laboratories with a W target was used to obtain the Laue pattern of the crystal. Raman spectroscopy was collected in the back-scattering configuration by a HR 800 system from Horiba JobinYvon, and a 532 nm laser was used as the excitation source. Scanning electron microscopy (SEM) was performed on a Hitachi S-4800 ultrahigh resolution (UHR) field emission (FE) SEM, and the images were obtained at an acceleration voltage of 5.0 kV. Transmission electron microscopy (TEM) images were obtained with a JEOL JEM-2100F transmission electron microscope operating at an acceleration voltage of 200 kV. Atomic force microscopy (AFM) was carried out with a Bruker Dimension Icon atomic force microscope.

Results and discussion

Owing to the high melting point of molybdenum disulfide and the volatility of sulfur, a tin (Sn) flux method was selected to grow bulk MoS_2 single crystals. Metallic Sn is a commonly-used flux due to its low melting point (232 °C) and high boiling point (2260 °C). Moreover, Sn has good solubility in acid, so the flux can be easily removed from the MoS_2 crystals.[28] The starting composition (Mo:S:Sn) and the growth temperature, which had great impact on the size and quality of MoS_2 crystals, had been determined by series of preliminary experiments. We found that the optimal conditions to produce MoS_2 crystals were as follows: growth temperature 1100-1150 °C, starting composition of Mo:S:Sn 1:2:10-1:2:15 (see Figure S1). The effect of the cooling rate on the size and morphology of the MoS_2 crystals was investigated in detail. In this work, the cooling rate was varied from 0.5 to 6 °C/h, and the obtained MoS_2 crystals are shown in Figure 1 (a)-(c).

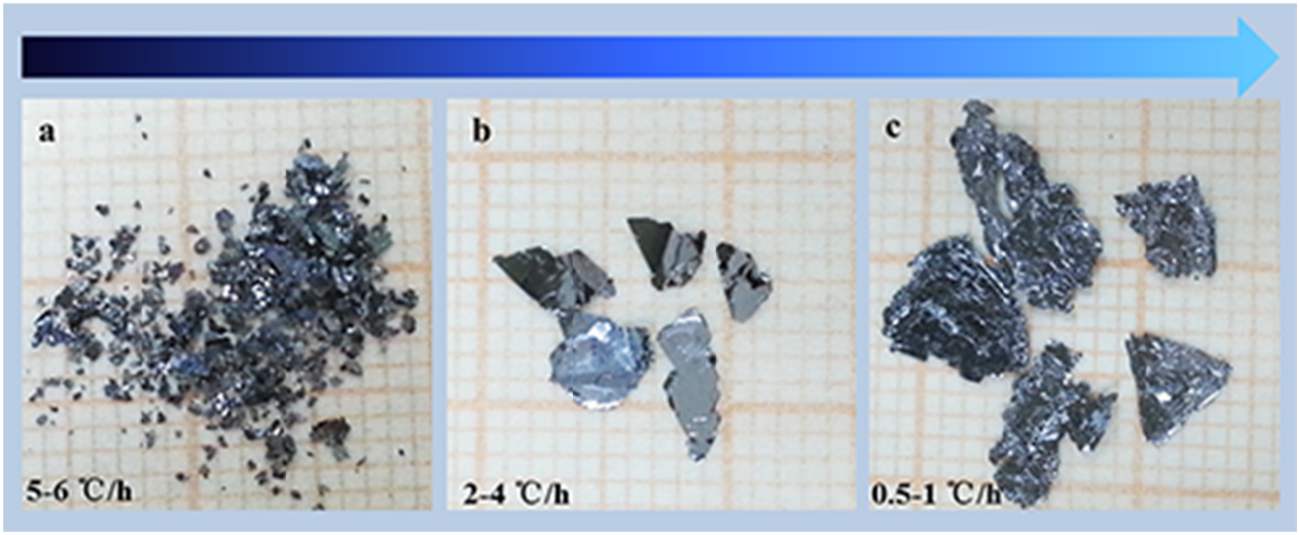

Figure 1. MoS_2 crystals grown by Sn flux method at a cooling rate of (a) 5-6 °C/h, (b) 2-4 °C/h, and (c) 0.5-1 °C/h. Each small square in all images is 1 mm^2.

The experiments reveal that the cooling rate has a great effect on the size and morphology of the MoS_2 crystals. At a quicker cooling rate of 5-6 °C/h, a number of small-sized crystal chips produced, as shown in Figure 1a. When the cooling rate was decreased to 2-4 °C/h, the size of crystals increased to 3-5 millimeters, and the crystalline quality improved obviously (Figure 1b). When the cooling rate was further decreased to 0.5-1 °C/h, and the size of crystals further increased. However, it is determined that samples obtained were polycrystalline MoS_2 (Figure 1c). This result may involve a complicated crystallization process that should include more influence factors. In conclusion, highly crystalline large-sized crystals can be obtained by using a cooling rate of 2-4 °C/h in these experiments. As is shown in Figure 2a, the Sn flux method enables a

scalable low cost solution to the production of highly crystalline bulk clear MoS_2 single crystals with a smooth large-sized area.

In order to characterize the crystalline quality of the bulk MoS_2 single crystals that were grown, we carried out X-ray diffraction (XRD) and Laue measurements. Figure 3 shows the XRD patterns of MoS_2 flakes and their powder. The MoS_2 powder pattern agrees well with the theoretically calculated one (Figure 3b), while only the [00l] diffraction lines were visible for the MoS_2 flakes, indicating that the surface of the crystals lies in the crystallographic *ab*-plane due to its strong two dimensional growth habit. Figure 2b shows a typical Laue diffraction pattern with hexagonal symmetry, and the clear and bright diffraction points indicate that the bulk MoS_2 single crystals grown by Sn flux method are of high crystalline quality.

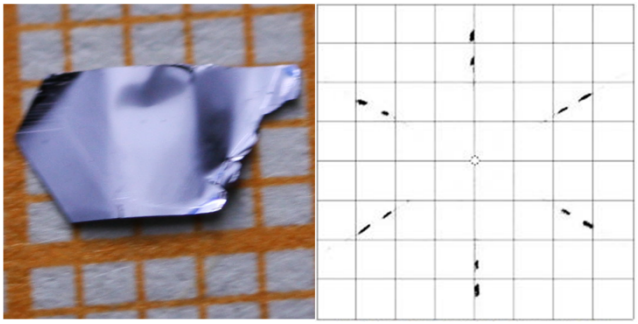

Figure 2. (a)Highly crystalline bulk MoS_2 single crystal grown by Sn flux method at a cooling rate of 2 °C/h. The crystal size is about 3 mm × 5 mm. (b) Laue pattern of bulk MoS_2 single crystal grown by Sn flux method at a cooling rate of 2 °C/h.

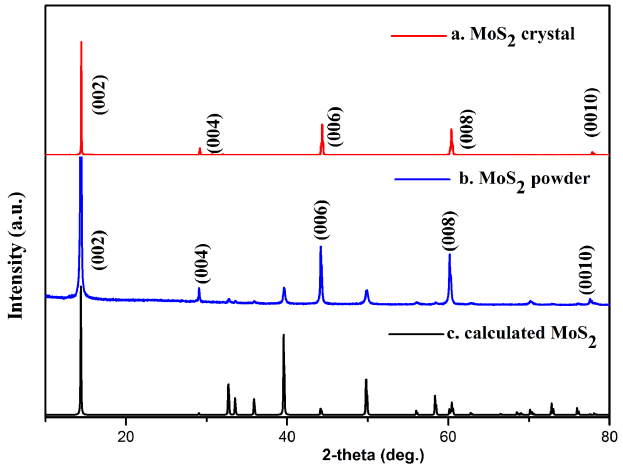

Figure 3. XRD pattern of (a) MoS_2 crystals, (b) MoS_2 powder ground from grown crystals, and (c) calculated.

Figure 4 shows a typical Raman spectrum of MoS_2 grown by the Sn flux method. Hexagonal MoS_2 belongs to the $D^4_{6h}(P6_3/mmc)$ group, and contains two molecular units with a total of six atoms within the unit cell.[29] There are twelve modes of lattice vibration: $A_{1g}+2A_{2u}+2B_{2g}+B_{1u}+E_{1g}+2E_{1u}+2E_{2g}+E_{2u}$, among which only four are Raman active (A_{1g}, E_{1g}, E^2_{1g}, E^2_{2g}).[29, 30] The A_{1g} mode corresponds to in-plane vibration involving the S atoms (408 cm^{-1}), while the E^1_{2g} mode relates to out-of-plane vibration of the Mo and S atoms (383 cm^{-1}).[29-31] The weaker peak at 453cm^{-1} is due to a secondary phonon mode 2LA(M).[31] For the as-grown crystal, the other two modes (E_{1g}, E^2_{2g}) could not be detected due to selection rules for scattering geometry (E_{1g})[30] or because the energy (E^2_{2g}) was below our measurement range.

SEM measurements were used to further characterize the MoS_2 crystals grown under the optimal growth parameters. In Figure 5(a,b), the surface of the crystals appear clean and smooth, and no obvious defects are observed. From EDS results (see Figure S2), one can conclude that no trace of the Sn flux was present in the as-grown crystals. The high magnification (Figure 5a) shows the sharp 120 ° angles, in accordance with the six-fold symmetry of the crystal structure. According to the periodic bond chain (PBC) theory,[32] the direction of strongest chemical bonds is considered to be the fastest growth direction in the crystal. In the MoS_2 crystal structure, the covalent bonds in the *c*-plane are much stronger than the van der Waals forces perpendicular to the *c*-plane, and so the growth of MoS_2 crystals in the *c*-plane proceeds at a much faster rate than that along a direction that is perpendicular to the *c*-plane. This situation leads to a layered structure with a sequence of flats (~0.5−1μm thick) stacked along the *c*-axis.

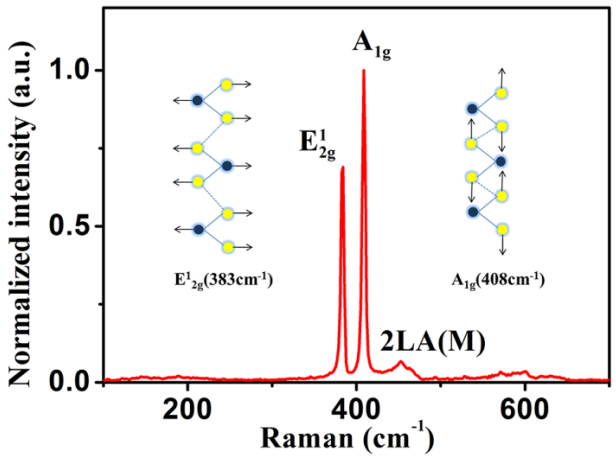

Figure 4. Raman spectrum of MoS_2 at room temperature. The A_{1g} mode corresponds to in-plane vibration involving S atoms (408 cm^{-1}), while the E^1_{2g} mode relates to out-of-plane vibration of Mo and S atoms (383 cm^{-1}). The weaker peak at 453cm^{-1} is due to a secondary phonon mode 2LA(M).

It has been confirmed that high quality MoS_2 crystals can be obtained at a cooling rate of 2-4 °C/h. The morphology and growth mechanism of MoS_2 crystals grown under these conditions were investigated by using AFM. According to classical crystal growth theory[33], there are three basic kinds of growth mechanism, including SDD[34], layer-by-layer (LBL) and dendritic growth. The growth preference depends on the degree of supersaturation. Generally at low supersaturation, SDD growth is dominant. Screw dislocation defects can provide self-perpetuating active edges that serve as nucleation sites to promote crystal growth at low supersaturation. Recently, some researchers have also reported SDD growth in Bi_2Se_3,[33] WSe_2[35] and MoS_2[36] nanosheets by CVD at a low supersaturation.

Through observation by optical microscope, we found that the surface of the MoS_2 crystals exhibited hexagonal screw dislocation steps, and the magnified screw dislocation steps were characterized by AFM in Figure 5c. The clear AFM image implies that screw dislocations with multiple Burgers vectors are produced in the Sn

flux system, and the dislocations then serve as step sources that promote continued crystal growth. The step sources do not disappear in the process of crystal growth and so form spiral tracks on the crystal surface. We measured the step height h and terrace width λ to describe the growth ledges. The height profile (Figure 5d) was measured by AFM along the red dashed line shown in Figure 5c. The step height h varies from 0.9 to 4 nm, and the terrace width is about 1-2μm. The basic step with a height of 0.9 nm is approximately equal to the thickness of a MoS_2 single layer (0.65 nm). According to Burton-Cabrera-Frank (BCF) theory,[37, 38] the lateral step velocity V_s, the growth rate normal to the surface R_m, and the slope $p = h/\lambda = R_m / V_s$ are closely related to the degree of supersaturation. In the flux growth system, the amount of supersaturation may fluctuate during the growth process, resulting in a change in V_s and R_m, and adjacent steps could bunch together to form a single step. Consequently, steps with inconsistent heights and widths appear on the surface of the crystals, as shown in Figure 5d.

Considering the application of the crystals for use in devices, we exfoliated the as-grown MoS_2 crystals by liquid-phase exfoliation in ethanol, and ultrathin sheets were prepared for characterization. In a low-magnification transmission electron microscopy (TEM) image (Figure 6e), the entire field of view shows the large ultrathin film, and some folds are visible, which reveal high flexibility and thinness. More detailed information can be obtained from high-resolution images (Figure 6a,b,c). Uniform atomic orientation and spacing demonstrate that an individual sheet consists of a single crystal domain. The electron diffraction image (Figure 6d) clearly shows the typical six-fold symmetry characteristic of MoS_2 with no redundant diffraction points, indicating a well-crystallized structure for the exfoliated MoS_2 sheet. Moreover, the morphology and thickness of the MoS_2 sheets was investigated with AFM (see Figure 6f). The height profile diagram (Figure 6g) indicates that the MoS_2 sheets consist of about 4 layers, since the height of a single layer is 0.65 nm.

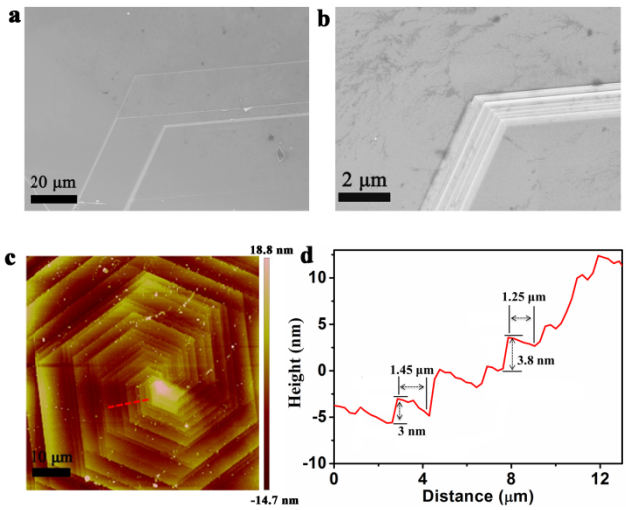

Figure 5. (a,b) SEM images of MoS_2 crystals grown at a cooling rate of 2 °C/h. (c) AFM image of screw dislocation steps on MoS_2 crystal surface. (d) AFM height profile of hexagonal screw dislocation steps along red dashed line in (c), step thickness is 1-4 nm, and terrace width is 1-2μm.

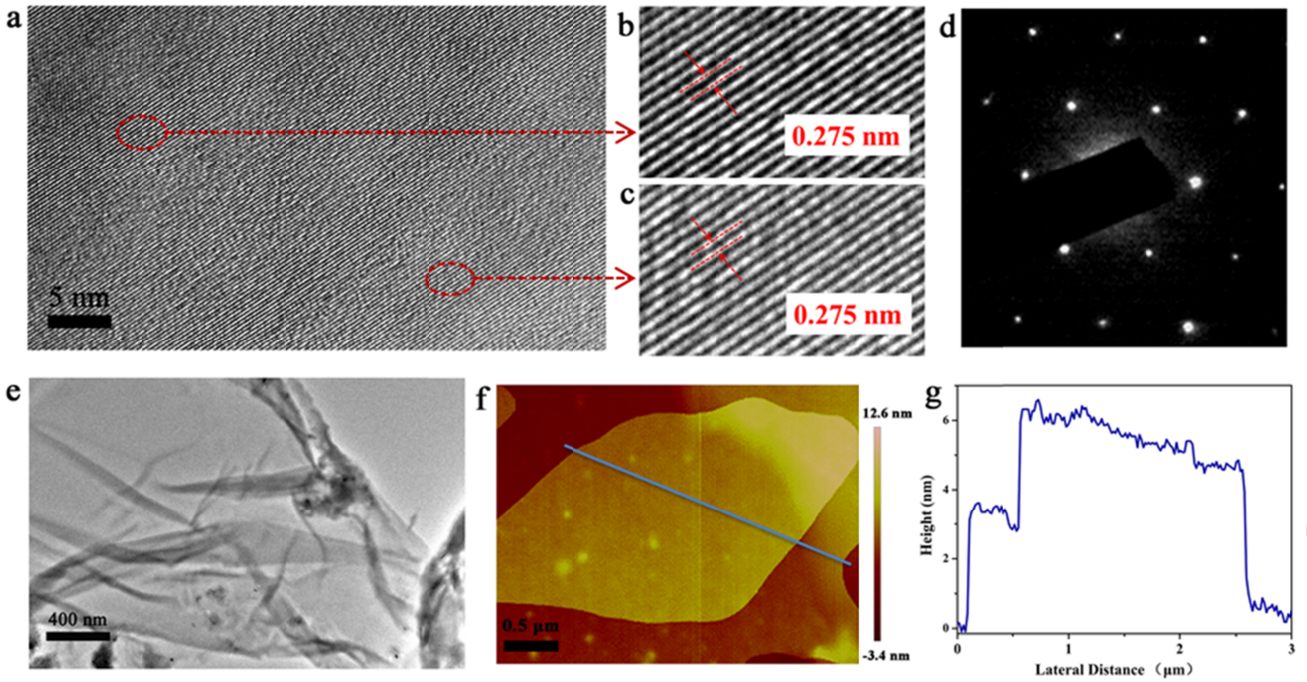

Figure 6. (a) high-resolution image of MoS_2 sheet exfoliated by liquid-phase exfoliation. (b,c) selected area high-resolution enlarged images of (a).(d) electron diffraction pattern of MoS_2 sheet. (e)Low-magnification TEM image of MoS_2 sheet (f) AFM image of MoS_2 sheets exfoliated from as-grown crystals by liquid-phase exfoliation method. (g) height profile of the few-layer MoS_2 sample in (f)

Passive Q-switching is achieved by placing a saturable absorber inside the laser resonator, then the loss of the cavity can be modulated by employing the saturated absorption characteristics of the saturable absorber.[39] The 2D semiconductor materials, including MoS_2, show a simple dual energy band structure of the conduction and the valence bands. Incident light with energy higher than the gap can excite carriers from the valence band to the conduction band. If the excitation has stronger intensity, all possible initial states are

depleted and the final states are partially occupied in accordance with the Pauli blocking effect such that the absorption will be saturated. As a consequence, when a high-quality MoS_2 nanofilm is inserted into a laser cavity, the laser will be modulated and changed from continuous wavelength operation to pulsed operation.[40 41] The ultrathin MoS_2 sheets exfoliated from as-grown crystals, were used as MoS_2 saturable absorbers（ SA）in a solid state laser. The as-prepared ultrathin MoS_2 suspension was uniformly applied dropwise onto the ultraviolet quartz glass substrate to serve as the saturable absorber mirror in the laser experiment. The passively Q-switched laser experiment was conducted with the setup shown in Figure 7. Using the MoS_2 SA, a passively Q-switched laser at a wavelength of 1.06 μm, was operated with a Nd:YVO_4 crystal as gain medium. The pulse width and repetition rate of the passively Q-switched laser were measured with a digital oscilloscope. Typical pulses are shown in Figure 8 with pulse width of 326 ns. When an incident pump power is 4 W, the maximum output power of the laser was 250 mW, a maximum repetition rate of 524 kHz and a single pulse energy of 0.48 μJ. The pulse width obtained in our experiment is narrower than that reported elsewhere in the literature[11] using PLD prepared MoS_2 as the SA. The laser results demonstrate that ultrathin MoS_2 exfoliated from the flux-grown MoS_2 crystals is a promising candidate for use as the saturable absorber for Q-switched SSLs.

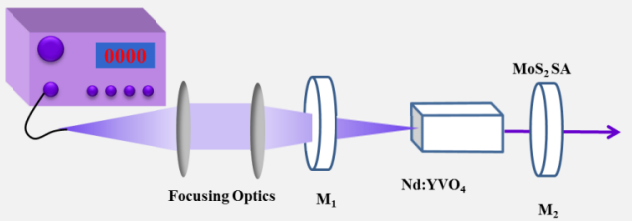

Figure 7. Schematic diagram of passively Q-switched experimental set-up

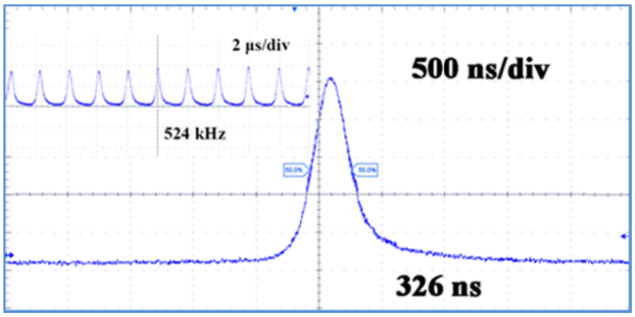

Figure 8. Q-switched pulse profile with pulse width of 326 ns, Inset: corresponding spectrum centered at 1.06 μm, pulse trains with repetition rate of 524 kHz recorded at 2 μs per division.

Conclusions

In conclusion, we have reported on a novel Sn flux method that can be used to grow bulk MoS_2 crystals. It can be widely extended to the growth of other TMDCs materials. Bulk MoS_2 single crystals with dimensions of 3 mm × 5 mm were successfully grown by the Sn flux method. The morphology and size of the MoS_2 crystal can be controlled by adjusting the cooling rate during crystal growth. The screw dislocation steps that appeared suggested that MoS_2 crystals grown by the Sn flux method follow a screw-dislocation-driven (SDD) growth mechanism. From the bulk crystals, highly crystalline large-scale MoS_2 films were obtained by the method of liquid-phase exfoliation. Ultrathin MoS_2 films were used as a Q-switching element in laser experiments, with the resulting pulses having a width of 326 ns, a maximum output power of 250 mW, and a single pulse energy of 0.48 μJ

Acknowledgment.

The authors appreciate the help of Dr. R. I. Bougton (Bowling Green State University) for revising the manuscript. The authors also gratefully acknowledge financial support by the National Natural Science Foundation of China (Grant Nos. 51321091, 51227002, 51272129 and 51323002), Shandong Provincial Natural Science Foundation, China (ZR2014EMM015), National Laboratory for Infrared Physics (Z201401), and the Program of Introducing Talents of Disciplines to Universities in China (111 Program No. b06015).

Notes and references

[1]State Key Laboratory of Crystal Materials, Shandong University, Jinan, 250100, China
[2]Key Laboratory of Functional Crystal Maerials and Device (Shandong University, Ministry of Education), Jinan, 250100, China

Corresponding Author

Xutang Tao：txt@sdu.edu.cn; Shanpeng Wang: wshp@sdu.edu.cn.

1 M. Chhowalla, H. S. Shin, G. Eda, L.-J. Li, K. P. Loh and H. Zhang, *Nature chemistry*, 2013, 5, 263-275.
2 Q. H. Wang, K. Kalantar-Zadeh, A. Kis, J. N. Coleman and M. S. Strano, *Nature nanotechnology*, 2012, 7, 699-712.
3 H. Wang, H. Feng and J. Li, *Small*, 2014, 10, 2165-2181.
4 B. Radisavljevic, A. Radenovic, J. Brivio, V. Giacometti and A. Kis, *Nature Nanotechnology*, 2011, 6, 147-150.
5 N. Huo, S. Yang, Z. Wei, S.-S. Li, J.-B. Xia and J. Li, *Sci. Rep.*, 2014, 4, 5209.
6 Z. Yin, H. Li, H. Li, L. Jiang, Y. Shi, Y. Sun, G. Lu, Q. Zhang, X. Chen and H. Zhang, *ACS nano*, 2011, 6, 74-80.
7 H. Hwang, H. Kim and J. Cho, *Nano Lett.*, 2011, 11, 4826-4830.
8 K. Chang and W. Chen, *ACS Nano*, 2011, 5, 4720-4728.
9 D. Voiry, H. Yamaguchi, J. Li, R. Silva, D. C. Alves, T. Fujita, M. Chen, T. Asefa, V. B. Shenoy and G. Eda, *Nature materials*, 2013, 12, 850-855.
10 K. F. Mak, C. Lee, J. Hone, J. Shan and T. F. Heinz, *Phys. Rev. Lett.*, 2010, 105, 4.
11 S. Wang, H. Yu, H. Zhang, A. Wang, M. Zhao, Y. Chen, L. Mei and J. Wang, *Adv. Mater.*, 2014, 26, 3538-3544.
12 R. Frindt, *Journal of Applied Physics*, 1966, 37, 1928-1929.
13 P. Joensen, R. Frindt and S. R. Morrison, *Materials research bulletin*, 1986, 21, 457-461.
14 J. N. Coleman, M. Lotya, A. O'Neill, S. D. Bergin, P. J. King, U. Khan, K. Young, A. Gaucher, S. De and R. J. Smith, *Science*, 2011, 331, 568-571.
15 Y. H. Lee, X. Q. Zhang, W. Zhang, M. T. Chang, C. T. Lin, K. D. Chang, Y. C. Yu, J. T. W. Wang, C. S. Chang and L. J. Li, *Adv. Mater.*, 2012, 24, 2320-2325.
16 S. Balendhran, J. Z. Ou, M. Bhaskaran, S. Sriram, S. Ippolito, Z. Vasic, E. Kats, S. Bhargava, S. Zhuiykov and K. Kalantar-Zadeh, *Nanoscale*, 2012, 4, 461-466.
17 J. Zheng, H. Zhang, S. Dong, Y. Liu, C. T. Nai, H. S. Shin, H. Y. Jeong, B. Liu and K. P. Loh, *Nature communications*, 2014, 5, 2995.
18.Y. H. Lee, X. Q. Zhang, W. J. Zhang, M. T. Chang, C. T. Lin, K. D. Chang Y. C. Yu, J. T. W. Wang, C. S. Chang, L. J. Li and T. W. Lin, *Adv. Mater.*, 2012, 24, 2320-2325.
19 W. Zhou, X. Zou, S. Najmaei, Z. Liu, Y. Shi, J. Kong, J. Lou, P. M. Ajayan, B. I. Yakobson and J.-C. Idrobo, *Nano Lett.*, 2013, 13, 2615-2622.
20 J. N. Coleman, M. Lotya, A. O'Neill, S. D. Bergin, P. J. King, U. Khan, K. Young, A. Gaucher, S. De, R. J. Smith, I. V. Shvets, S. K. Arora, G. Stanton, H. Y. Kim, K. Lee, G. T. Kim, G. S. Duesberg, T. Hallam, J. J. Boland, J. J. Wang, J. F. Donegan, J. C. Grunlan, G. Moriarty, A. Shmeliov, R. J. Nicholls, J. M. Perkins, E. M. Grieveson, K. Theuwissen, D. W. McComb, P. D. Nellist and V. Nicolosi, *Science*, 2011, 331, 568-

571.
21 S. Balendhran, J. Z. Ou, M. Bhaskaran, S. Sriram, S. Ippolito, Z. Vasic, E. Kats, S. Bhargava, S. Zhuiykov and K. Kalantar-Zadeh, *Nanoscale*, 2012, 4, 461-466.
22 A. Ubaldini, J. Jacimovic, N. Ubrig and E. Giannini, *Crystal Growth & Design*, 2013, 13, 4453-4459.
23 H. J. Scheel, *Journal of Crystal Growth*, 1974, 24–25, 669-673.
24 R. S. Chen, C. C. Tang, W. C. Shen and Y. S. Huang, *Nanotechnology*, 2014, 25.
25 H. Zhang, S. Lu, J. Zheng, J. Du, S. Wen, D. Tang and K. Loh, *Optics Express*, 2014, 22, 7249-7260.
26 K. Wang, J. Wang, J. Fan, M. Lotya, A. O'Neill, D. Fox, Y. Feng, X. Zhang, B. Jiang and Q. Zhao, *ACS nano*, 2013, 7, 9260-9267.
27 B. Xu, Y. Cheng, Y. Wang, Y. Huang, J. Peng, Z. Luo, H. Xu, Z. Cai, J. Weng and R. Moncorgé, *Optics Express*, 2014, 22, 28934-28940.
28 M. G. Kanatzidis, R. Pöttgen and W. Jeitschko, *Angewandte Chemie International Edition*, 2005, 44, 6996-7023.
29 T. Wieting and J. Verble, *Phys. Rev. B*, 1971, 3, 4286.
30 J. Verble and T. Wieting, *Phys. Rev. Lett.*, 1970, 25, 362.
31 X. Zhang, W. Han, J. Wu, S. Milana, Y. Lu, Q. Li, A. Ferrari and P. Tan, *Phys. Rev. B*, 2013, 87, 115413.
32 P. Hartman and P. Hartman, *Crystal growth: an introduction*, North-Holland Publishing Company, 1973.
33 A. Zhuang, J. J. Li, Y. C. Wang, X. Wen, Y. Lin, B. Xiang, X. Wang and J. Zeng, *Angewandte Chemie*, 2014, 126, 6543-6547.
34 W. K. Burton, N. Cabrera and F. C. Frank, *Philosophical Transactions of the Royal Society of London. Series A, Mathematical and Physical Sciences*, 1951, 243, 299-358.
35 L. Chen, B. Liu, A. N. Abbas, Y. Ma, X. Fang, Y. Liu and C. Zhou, *ACS nano*, 2014, 8, 11543-11551.
36 L. Zhang, K. Liu, A. B. Wong, J. Kim, X. Hong, C. Liu, T. Cao, S. G. Louie, F. Wang and P. Yang, *Nano Lett.*, 2014, 14, 6418-6423.
37 W.-K. Burton, N. Cabrera and F. Frank, *Philosophical Transactions of the Royal Society of London. Series A, Mathematical and Physical Sciences*, 1951, 299-358.
38 W. Burton, N. Cabrera and F. Frank, *Nature*, 1949, 163, 398-399.
39 W. Koechner, *Solid-State Laser Engineering*, Springer, 2006.
40 S. Wang, H. Yu and H. Zhang, *Photon. Res.*, 2015, 3, A10-A20.
41 R. I. Woodward, R. C. T. Howe, G. Hu, F. Torrisi, M. Zhang, T. Hasan and E. J. R. Kelleher, *Photon. Res.*, 2015, 3, A30-A42.